JET–P(99)32

C Gowers et al

A Comparison of a Streak Camera and MCP Photomultipliers for High Resolution Lidar Thomson Scattering

JET–P(99)32

A Comparison of a Streak Camera and MCP Photomultipliers for High Resolution Lidar Thomson Scattering

C Gowers, S Ali-Arshad[1], P Nielsen[2].

JET Joint Undertaking, Abingdon, Oxfordshire, OX14 3EA,
[1]CERN CH-1211, Geneva 23, Switzerland.
[2]Consorzio RFX, Corso Stati Uniti, 4, 35127 Padova, Italy.

Preprint of a Paper to be submitted for publication in the proceedings of the
Laser-Aided Plasma Diagnostics Conference,
27th September–1st October 1999, Lake Tahoe, California, USA.

September 1999

ABSTRACT

To resolve the edge pressure gradient a spatial resolution of better than 1 cm is required at the toroidal mid-plane of the JET plasma. To obtain sufficient signal in Thomson scattering the scattering volume may be inclined at an angle to the poloidal flux surfaces (tangential). Due to access restrictions spatially resolved Thomson scattering at JET uses the time-of-flight LIDAR technique. Spatial resolution down to 5 cm has been demonstrated using this technique. By scattering off regions of large poloidal flux expansion this can be equivalent to less than 1 cm at the mid-plane. Two systems are described, one using a streak camera, for maximum spatial resolution, and one using MCP-photomultipliers. The reason for the better performance of the second system and possible future upgrades are briefly discussed.

1. INTRODUCTION

To resolve the electron temperature and density in the edge region even on a tokamak plasma as large as that in JET requires a spatial resolution of 1 cm or less. Spatially resolved Thomson scattering offers the unique opportunity of measuring simultaneously the gradients of both electron temperature and electron density. Mainly due to access restrictions the scattering systems at JET use a time-of-flight or LIDAR (light detection and ranging) principle to provide profile information[1] but the method also has some other significant advantages. Figure 1 shows a cross section of the JET Divertor/Edge Thomson Scattering System. Only a single (large) window or window assembly is required for both laser input and backscattered light collection, and it uses the same set of detectors for all scattering positions. This reduces the calibration problem particularly with respect to the density profile. Two detection systems, a streak camera based system and a scheme using microchannel plate (MCP) photomultipliers are compared and contrasted in this paper.

2. GENERAL DESCRIPTION

The best possible spatial resolution by either of the detector systems is 5 cm (see below). With access from the main horizontal port the laser is aimed at a point 0.2 - 0.3 m above the X-point of a typical divertor plasma. This gives an equivalent mid-plane penetration of 5 - 10 cm inside the last closed flux surface (LCFS) Fig 1. The angle of the laser beam with respect to the LCFS at the outboard side is ~ 30 degrees which together with the flux expansion gives a mid-plane equivalent resolution across the flux surfaces of 3-5 times better than the spatial resolution along the line of sight.

The spatial resolution, ΔL, of a LIDAR system is given by: $\Delta L = [(\tau^2_L + \tau^2_d + \tau^2_r)^{1/2}]_* c/2$ where c is the speed of light and τ_L , τ_d and τ_r are the laser pulse length and the response times of the detector and the recording system respectively. The pulse length of the ruby laser used is 300 ps which immediately limits the spatial resolution to ~5 cm. Using a streak camera a resolution of this order is achieved. Using the same detectors and a 1 GHz recording system as in the main LIDAR system gives a spatial resolution of about 12 cm.

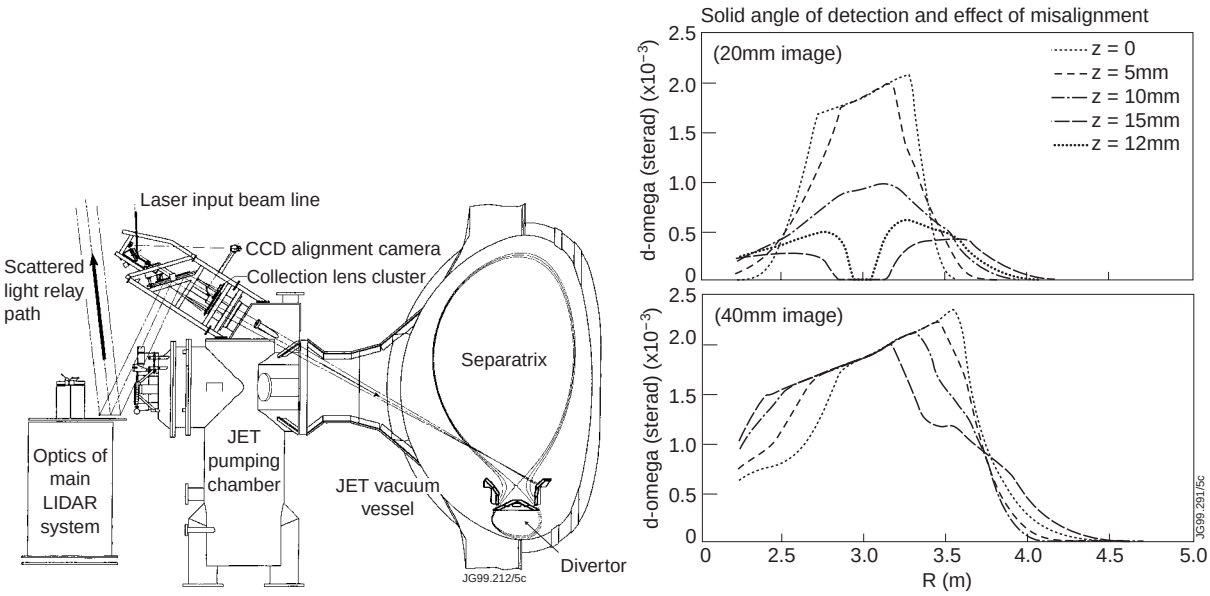

Figure 1 (left) General layout of LIDAR Thomson scattering system used for both edge measurements. The laser beam and the collected light are both passing through a penetration in the Torus Hall biological shield and a window cluster on top of the pumping box. Alignment is achieved by looking at the image on the divertor tile of a 633 nm alignment beam using a CCD camera inside the spectrometer; (upper right) vignetting curve for streak camera system and (lower right) for MCP photomultiplier system. The effect of misalignment (z) of the laser beam is also shown.

The vacuum window viewing this path is a cluster of 7 windows approximately 4 m away from the central scattering volume. The central window is used for passing the laser beam and the 6 surrounding windows are used for collecting the scattered light. The effective F# of the collection system seen from the scattering volume is ~20. The subtended F# is ~14. The laser beam waist at the centre of scattering is ~5 mm. However, in a LIDAR system the solid angle of collection varies with scattering position. We call this “the vignetting curve”. The scattering length over which we can make useful measurements is limited by how much the collection throughput exceeds the minimum required étendue of a single point system.

3. THE STREAK CAMERA SYSTEM

In order to get maximum spatial resolution we would like to choose a detector with a response time of less than 300 ps. A streak camera offers this and the streak camera chosen was a Thomson CSF, TSN 506. The capability of the streak camera solution was demonstrated earlier[1] in a system running parallel to the main LIDAR system. The length of the chord through the plasma is ~1.5 m. To cover a significant fraction of this scattering length we have to choose the slowest sweep speed (150 ps/mm), giving an overall sweep time of 5.4 ns, corresponding to 80 cm scattering length.

Choosing an input spot size of 3 mm (photocathode size) gives an overall temporal resolution of 380 ps and a spatial resolution of 7 cm. A spot size of 3 mm using F/2 optics translates into an étendue, limited by the streak camera only, of 1.4 mm^2 x sterad. We can think of this as

a limiting aperture at the central scattering location with a diameter of ~20 mm. With this assumption and otherwise ideal relay optics we can calculate the resulting "vignetting curve", Fig 1 (top right). The figure shows the vignetting curve for perfect alignment of the laser beam to the centre of the collection system. With perfect alignment we get the expected $1/R^2$ dependence around the central scattering position, where R is the distance to the window, and the total length of the scattering region matches the total sweep length of the streak camera. However, as the figure shows, the system is very sensitive to small misalignments, which must be known and corrected for to obtain the true density profile.

The photons from the P11 phosphor of the streak tube screen are amplified by a single stage gated image intensifier with a luminous gain of $\sim 10^4$. The output of the intensifier is in turn imaged by a F/1.2 camera lens onto a thermoelectrically cooled CCD camera (J Wright). The gain of the system is sufficiently high that the effective quantum efficiency is essentially given by the extended red (S25) photocathode of the streak tube, with a low excess noise factor. The quantum efficiency of the streak camera was measured to be 3% at 700 nm. The resulting noise factor is likely to be of order 3 to 4 but has not been explicitly determined.

Intense stray laser light pulses outside the streak period produce stray electrons inside the tube which corrupt the image on the phosphor. To prevent this from happening, the streak tube was gated off using a grid (aperture plate), 7 mm from the photocathode. The applied gate pulse to the grid has a duration of 10 ns with a rise and fall time of less than 2 ns. Gating off must begin ~3 ns before the laser pulse reaches the divertor tiles. This means that we cannot measure nearer to them than 0.5 m. In addition, any gate induced variation in transit time of the photoelectrons as they traverse from photocathode to grid must be taken into account via a sweep linearity measurement (see below).

3.1. Collection Optics and Spectrometer

The ruby laser and the streak camera are both located outside the biological shielding wall. The total distance from laser to detector is ~ 100 m. To pass the scattered signal arriving at the viewing window to the spectrometer we use an optical relay system consisting of 6 mirrors and 5 AR-coated lenses. The mirrors have either broad band dielectric coatings or protected silver coatings for maximum transmission.

The expected temperature range for the diagnostic was 50-1000 eV. For this range a Littrow mounted, f=0.5m, F/3.3 grating instrument covering 600-700 nm was designed. This used a 1200 lines/mm grating with an efficiency for both polarizations of >70% and a single LaK10 lens. The input aperture was 5 mm diameter, giving a spectral resolution of ~10 nm. Two notch filters (Kaiser Optical Systems) were required in front of the input aperture, one filter to suppress the ruby laser stray light and one to suppress the H-alpha light. The overall transmission of the optical train including the spectrometer was T ~ 0.1.

3.2. Results

Figure 2 shows an example of a successful measurement. Top centre is the raw signal as recorded by the CCD camera, time is along the horizontal axes and spectrum along the vertical axes. The top of the picture shows three time markers. These are derived by letting a small fraction of the ruby laser pulse bounce between two near perpendicular, 95% reflectivity mirrors, 15 cm apart. The repeated, 1 ns apart, pulses are imaged onto a fibre which illuminates the spectrometer output slit at a location corresponding to 700 nm. The recording of these pulses allowed us to determine the absolute time of the scattered signal with respect to the laser pulse and to correct for transit time induced variations of the sweep rate. We also note the two dark bands at the ruby wavelength and at H-alpha resulting from the notch-filters, the time markers are located in the ruby band. The fitted electron temperature and density profiles along the line of sight are shown on the right of Fig.2. Transforming the results to the equivalent position at the equatorial plane yields a temperature gradient of ~500eV/cm. As expected, the equatorial data show good agreement for the fitted electron temperatures on the same flux surface as we pass along the scattering chord. The density fits do not generally show the same agreement. To determine the density requires absolute calibration and the exact knowledge of the solid angle as function of position (vignetting curve). As indicated earlier this curve is subject to change from small variations of the alignment.

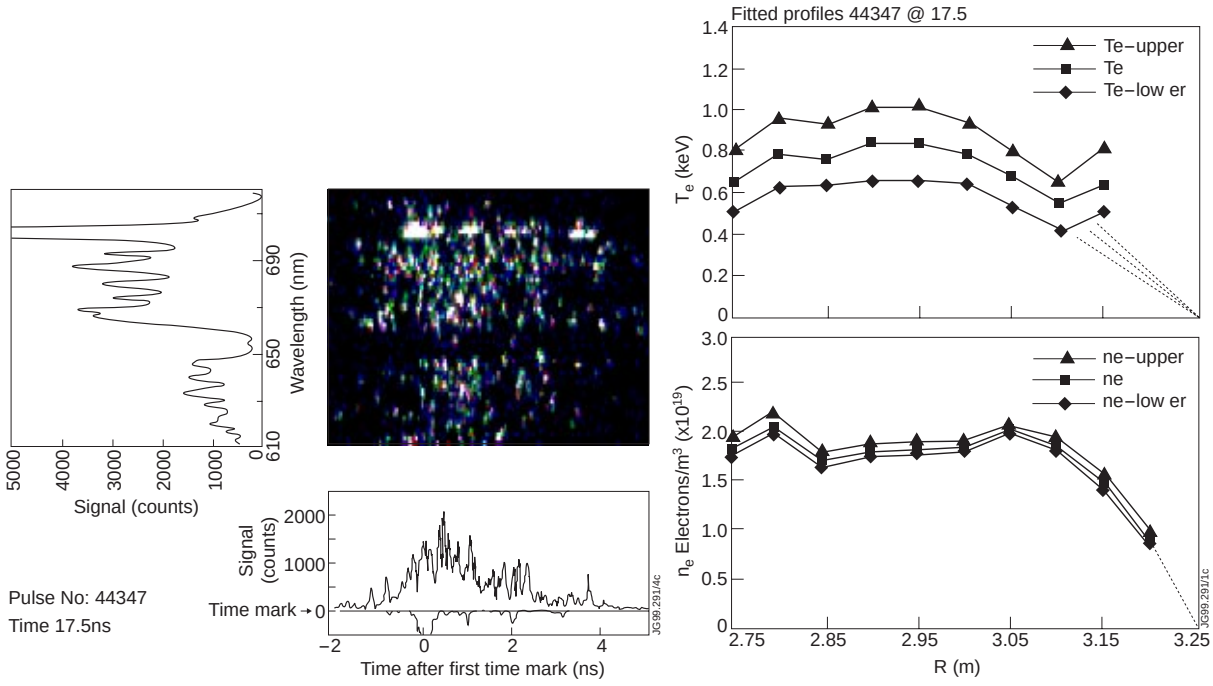

Figure 2 (top centre) Streak camera signal recorded by CCD camera, (bottom centre) integrated intensity vs. time and time marks, (top left) integrated spectrum. (right) Fitted temperature and density profiles along sight line.

In spite of the potential 0.5 ns resolution the number of photoelectrons is too low to make a meaningful analysis on this time scale. Fitting is therefore performed by adding data from 1 ns time slices. Even then the temperature data exhibits significant uncertainty caused by the low

signal intensity. The problem of low intensity is further exacerbated by the narrow vignetting curve. Towards the plasma edge where the density is decreasing the signal is further decreased through vignetting. The effective 15cm spatial resolution gives an excellent equivalent equatorial resolution for the point of tangency and even at the plasma edge we have a resolution of the order of a few centimetres. Because of the limited sweep length it was not possible to determine any background light level. In general this did not appear to cause a problem except for a few very high density cases where background clearly affected the fit.

The spectral calibrations, wavelength calibration and slitfunction, are performed in the laboratory outside the Torus Hall biological shield. The more important calibration, measuring the vignetting curve, was achieved by using either Rayleigh or Raman scattering when the JET vacuum vessel was open to atmospheric air pressure.

4. MCP-PHOTOMULTIPLIER SYSTEM

Two improvements were required to significantly improve the system, a longer scattering length and a stronger signal. As we have described above the scattering length for the given vacuum vessel window is given by the size of the detector. To get a significantly larger detector we considered using MCP-photomultipliers. 10 mm diameter MCP-photomultipliers have response times of ~ 200-300 ps, equivalent to the result obtained with the streak camera. The resulting image size of a 10 mm diameter detector in the central scattering position is 40 mm. The vignetting curve Fig.1 (lower right) now becomes more than 1.5 m long with a section ~0.75 m long without vignetting. The solid angle of collection over this length is a simple $1/R^2$ dependence. The larger image size also means that the vignetting curve over the central region is insensitive to misalignments of ~1 cm between laser beam and collection optics. The relay optical system was changed to accommodate the larger throughput. With the given optical arrangement the throughput is now limited by the size of the penetration in the biological shield, which also matches the 10 mm diameter detector.

To improve the signal strength we reduced the number of optical elements as much as possible and reviewed the transmission of all surfaces. The grating spectrometer was replaced by a 4 channel filter spectrometer similar to that used in the main LIDAR system.[1] The channel nearest the ruby wavelength has the ruby notch filter in front of the photocathode. The channel containing the H-alpha line has the H-alpha notch filter in front of the detector. No signal is transmitted through more than 3 filter reflections or transmissions. The resultant overall transmission from laser to detector is 20%, approximately twice that of the streak camera system. The photocathodes of the detectors are the same type as on the streak camera, S25. Higher quantum efficiency could be obtained by using Ga-As detectors and this is currently under consideration. The important “vignetting curve” is again measured using a Raman scattered signal from atmospheric pressure air in the torus when JET is shutdown.

4.1. Detectors and Excess noise factor

Three commercial MCP photomultipliers (Photek, Hamamatsu and ITT) have been assessed for this application. From response time measurements the detectors offered a spatial resolution for the system of 8 cm, 9 cm and 12 cm respectively. Even a resolution of 12 cm along the laser line of sight is still within the range of interest for the edge measurement. An important parameter determining the quality of the signal from a photomultiplier is its effective quantum efficiency, q_{eff}, calculated from the observed signal and noise characteristics. Our measurements of this parameter showed that although the photocathode quantum efficiencies were quoted as 5.5%, 7% and 5.2% their q_{eff} 's were 0.53%, 0.66% and 1.39%. High effective quantum efficiency is imperative in this application. The faster response times of the Photek and Hamamatsu tubes relative to the ITT tube does not make up for their much lower q_{eff}. The resulting gradient scale-length that can be measured with these tubes would not be better than the ITT tube due to a larger uncertainty in the measured electron temperature and density at a given point. We therefore decided to initially use the ITT MCP photomultipliers in the system. The resultant equivalent spatial resolution at the equatorial mid-plane is as we have seen a factor of 3-5 times better depending on the alignment.

In order not to charge deplete the micro-channel plates by the laser stray light pulses and the background light level, the detectors are only gated on for a duration of 25 ns. The gate pulse is applied to all detectors at the same time. The gate pulse is triggered by a photodiode which monitors the laser pulse. This still causes a small jitter between the laser pulse time and the oscilloscope time. To provide absolute timing we introduce via a fibre a small optical signal from the laser pulse onto one of the detectors (time marker). This pulse also shows the overall time response of the system.

4.2. Analysis and Results

Fig 3 (left) shows a typical example of the output from the four detectors. The full traces are 50 ns long. In the figure we have zoomed in on the scattered signals. The initial part of the visible traces indicate the plasma light levels before the laser pulse arrives inside the plasma. The signals go into saturation at ~ 47 ns. This is when the leading edge of the laser pulse starts to interact with the tiles in the divertor region. As the four detector signals are synchronized to each other, the electron temperature and density at a given point in space can be fitted by selecting the appropriate time slice of the four signals. Temperature and density are fitted at 5 cm intervals along the major radius, corresponding to ~2 points per spatial resolution element. Fig.3 (right) shows the result of such a fit interpreted as profiles at the equatorial mid-plane. The raw signals indicate that density and temperature profiles exhibit gradients that are approaching the instrument resolution. This observation is confirmed when repeating the measurement with shallower penetration into the plasma, b) and c) on the temperature and density fits.

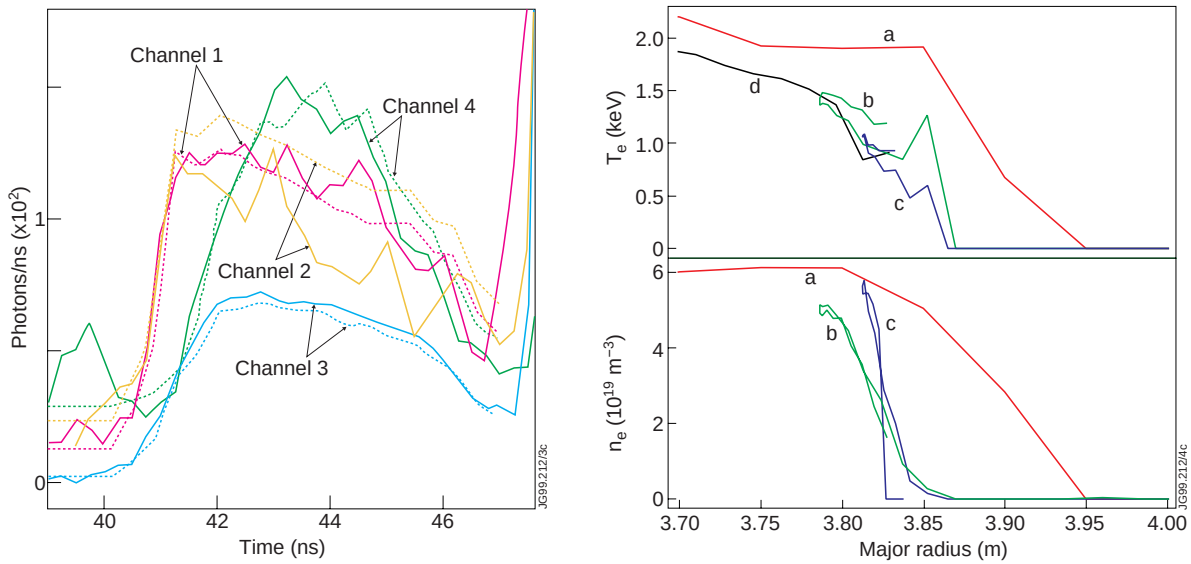

Figure 3. (Left) raw data for #47310, t=23.8s. The solid curves are the raw data and the dashed curves show the expected signal for the fitted T_e and n_e profiles. (Right) Resultant T_e and n_e profiles (b & c) for different levels of penetration (alignments) into the plasma compared with the main LIDAR system (a) and the ECE radiometer (d) profiles.

5. CONCLUSION

In the Divertor LIDAR Thomson scattering system at JET, significantly better measurement capability has been demonstrated with a combination of a filter spectrometer plus MCP-photomultiplier detectors than with the grating spectrometer/streak camera based system. The main improvement factors are the better “vignetting” performance obtained with the larger photocathodes available on the photomultipliers and the improved transmission of the somewhat simpler optical train when the filter spectrometer is used.

REFERENCES

[1] C. Gowers, B. W. Brown, H. Fajemirokun, P Nielsen, et al Rev. Sci. Inst. 66 471(1995)